



# Galaxy rotation curve based on RGB stars from the Gaia DR3 catalogue

P. N. Fedorov,<sup>1</sup>  A. M. Dmytrenko,<sup>2</sup> V. S. Akhmetov,<sup>2,3</sup>  A. B. Velichko,<sup>1</sup> V. P. Khramtsov,<sup>2</sup>  
S. I. Denyshchenko,<sup>1</sup> I. B. Vavilova,<sup>2</sup> D. V. Dobrycheva,<sup>2</sup> O. Sergijenko,<sup>2</sup> A. A. Vasylenko,<sup>2</sup>  
O. V. Kompaniiets<sup>2</sup>

<sup>1</sup>*Institute of astronomy of V.N.Karazin Kharkiv national university, Svobody sq. 4, 61022, Kharkiv, Ukraine*

<sup>2</sup>*Main Astronomical Observatory of the National Academy of Sciences of Ukraine, Akademik Zabolotnyi 27, Kyiv, 03143, Ukraine*

<sup>3</sup>*INAF-Osservatorio Astrofisico di Torino, Via Osservatorio 20, Pino Torinese, Turin, I-10025, Italy*

Accepted XXX. Received YYY; in original form ZZZ

## ABSTRACT

In this paper, we construct a detailed circular velocity curve of the Milky Way out to  $\sim 20$  kpc based on the radial component of the Jeans equation in cylindrical coordinates, assuming an axisymmetric gravitational potential, and show its dependence on azimuth. We use only *Gaia* DR3 data and aim to minimize the use of model data and various assumptions.

To build the rotation curves, we used a sample of 4,547,980 RGB stars with measured spatial velocities, covering the Galactic plane in the range of Galactocentric cylindrical coordinates  $150^\circ < \Theta < 210^\circ$  and  $0 < R < 20$  kpc. We exclude systematics in the data that may arise from neglecting higher-order moments of the velocity distribution and their dispersions, as well as due to random measurement errors in *Gaia*.

At the Sun's distance, the circular velocity  $V_c(R_0)$  turned out to be  $(229.63 \pm 0.30)$  km s<sup>−1</sup>, which is in good agreement with many previous estimates. The average slope of the circular velocity is  $(\sim -2.29 \pm 0.05)$  km s<sup>−1</sup> kpc<sup>−1</sup> obtained in the range of  $R$  from 6 to 20 kpc and  $\Theta$  from 150 to 210 degrees. The determined circular velocity curve has some peculiarities in behavior near  $R \sim 13$  and 18 kpc, but in general it does not contradict the results of other authors up to distances where our statistics are reliable.

**Key words:** methods: data analysis—proper motions—stars: kinematics and dynamics—Galaxy: kinematics and dynamics—solar neighborhood.

## 1 INTRODUCTION

The circular velocity curve  $V_c(R)$  of the Milky Way is usually constructed along the Galactocentric direction  $R$  passing through the Galactic centre and the Sun, using the axisymmetric Jeans equation that links the gravitational potential to the stellar kinematics encoded in the velocity–dispersion tensor. This procedure implicitly assumes that  $V_c(R)$  represents a global characteristic that may be extrapolated to the Galaxy as a whole. The justification for extrapolating the rotation curve throughout the Milky Way is the assumption of axial symmetry of the gravitational potential entering the Jeans equation. In practice, however, the available kinematic information covers only about one third of the Galactic disc, as observations cannot be obtained across the entire Galaxy. If the rotation curve varies with azimuth  $\Theta$ , then the classical approach to estimating the Galactic mass using an azimuthally averaged  $V_c(R)$  loses strict physical meaning.

The key assumptions underlying the Jeans equation, namely axial symmetry and dynamical equilibrium of the stellar population under study, are known to be violated, as demonstrated in numerous works (Fedorov et al. 2023; Akhmetov et al. 2024; Dmytrenko et al. 2023; Denyshchenko et al. 2024; Dmytrenko et al. 2025). These studies show that the distribution of azimuthal velocity components

of stellar centroids in the Galactic plane exhibits significant variations at different azimuthal angles, and that the Milky Way is neither strictly axisymmetric nor in dynamical equilibrium (Vasiliev et al. 2021; Antoja et al. 2018). Consequently, the determination of the circular velocity curve via the Jeans equation, and thus the inference of the Galactic mass, becomes strongly model-dependent. Current estimates of the Milky Way mass range from  $\sim 4 \times 10^{11} M_\odot$  to  $1.5 \times 10^{12} M_\odot$ , i.e. differing by more than a factor of three. This discrepancy arises not from an experimental error but from incomplete data and model assumptions.

A robust determination of  $V_c(R)$  requires precise kinematics for a sample containing a large number of stars with well-measured space velocities, ensuring statistically reliable results. *Gaia* data releases, being the largest and most precise available, have often been used to determine the circular velocity not only within the Solar neighbourhood but also at distances up to 20–30 kpc (Mróz et al. 2019; López-Corredoira & Sylos Labini 2019; Eilers et al. 2019; Chrobáková et al. 2020; Wang et al. 2023). However, two serious obstacles complicate this task. First, the precision of parallax-based distances deteriorates rapidly, especially beyond heliocentric distances of  $\sim 5$  kpc. Second, reaching such distances requires the use of intrinsically luminous stars, as only such stars are observable by *Gaia* at large ranges. Red giant branch (RGB) stars are therefore widely used as tracers in rotation-curve studies. Although RGB stars are useful tracers, their

\* E-mail: pnfedorov@gmail.com (PNF)

† E-mail: akhmetovvs@gmail.com (VSA)

observed velocities are affected by asymmetric drift, which systematically shifts the inferred circular velocity and is nontrivial to correct for.

Significant efforts have been devoted to mitigating the first limitation by improving the accuracy of *Gaia* parallaxes. For example, Lindegren et al. (2021) proposed parallax-correction functions. Eilers et al. (2019) used spectrophotometric parallaxes derived from APOGEE DR14 spectroscopy and multi-band photometry, while Mróz et al. (2019) utilised the Cepheid catalogue of Skowron et al. (2019). Bailer-Jones et al. (2021) introduced the so-called photogeometric distances combining a Galactic prior with astrometric data, and López-Corredoira & Sylos Labini (2019) proposed a distance-refinement method based on statistical deconvolution of parallax errors using the Lucy inversion algorithm (Lucy 1974).

To reduce the impact of asymmetric drift, many works apply restrictions such as excluding stars with  $|Z| > 1\text{--}2$  kpc, adopting  $\alpha$ -element enhancement cuts to separate thin- and thick-disc populations, or removing halo stars. These criteria reduce the influence of asymmetric drift but do not ensure its complete elimination. Moreover, such restrictions reduce the number of available stars, particularly at large distances, lowering the statistical robustness of the results.

The latest *Gaia* release, DR3 (Gaia Collaboration et al. 2021, 2023b), contains 32.2 million stars with radial velocities brighter than  $G_{\text{RVS}} \sim 14$ , with median radial-velocity precision ranging from  $1.3 \text{ km s}^{-1}$  at  $G_{\text{RVS}} \sim 12$  to  $6.4 \text{ km s}^{-1}$  at  $G_{\text{RVS}} \sim 14$ . Random proper-motion uncertainties are  $0.02\text{--}0.03 \text{ mas yr}^{-1}$  for  $G < 15$ ,  $0.07 \text{ mas yr}^{-1}$  at  $G = 17$ ,  $0.5 \text{ mas yr}^{-1}$  at  $G = 20$  and  $1.4 \text{ mas yr}^{-1}$  at  $G = 21$ . Parallax uncertainties have been reduced by a factor of 1.25. Using these data and the above mentioned distance-refinement approaches, circular-velocity curves have been extended to  $R \sim 25\text{--}30$  kpc (Ou et al. 2024; Zhou et al. 2023; Wang et al. 2023; Jiao et al. 2023; Koop et al. 2024). However, no consensus has yet been reached regarding the behaviour of the rotation curve at large radii: some works report a sharp, nearly Keplerian decline beyond  $\sim 15\text{--}25$  kpc, while others find an almost flat or slowly declining profile out to  $\sim 30$  kpc (e.g. Chrobáková et al. 2020). The reasons for discrepancies at large distances may be the non-stationarity of stellar systems, inaccurate selection of tracers, asymmetries, and inaccurate distances (Wang et al. 2023; McMillan et al. 2022). The applicability of the Jeans equation, with its assumptions of stationarity and symmetry, has therefore come under close examination (Koop et al. 2024), and many works introduce corrections or explicitly model disequilibria.

Despite these challenges, refining the Milky Way circular-velocity curve  $V_c(R)$  remains crucial, as it provides a practically useful approximation and plays an important role in many astrophysical applications. For instance, the shape of  $V_c(R)$  is used when comparing the Milky Way with external disc galaxies, since RC shapes reflect galaxy type. Most spiral galaxies display flat rotation curves at large radii, although some show declines, especially when traced with different indicators or at very low surface densities (Puglisi et al. 2023). Such comparisons help assess whether a possible downturn in the Milky Way rotation curve is unusual or typical.

The goal of the present study is to determine the Galactic rotation curve along different azimuthal directions using *Gaia* DR3 data alone, without any model-dependent inputs. A second objective is to derive the Galactic circular velocity using the Jeans equation with a minimal set of assumptions, employing all relevant velocity and dispersion moments corrected for *Gaia* measurement errors. The analysis is performed in spherical regions (bins) of radius 1 kpc, placed every 100 pc, enabling the construction of maps of all quan-

ties needed to evaluate the Jeans equation after removing potential systematics from the stellar velocity field.

## 2 DATA AND SAMPLE

In this study, we use RGB stars. Following Gaia Collaboration et al. (2023a), we identify RGB stars using the stellar-parameter criteria  $\log g < 3.0$  and  $3000 \text{ K} < T_{\text{eff}} < 5200 \text{ K}$ , as provided in Andrae et al. (2023). This selection yields a total of 10 976 663 sources. Among them, 5 913 442 stars have radial velocities reported in *Gaia* DR3.

As in our previous works (Fedorov et al. 2023; Dmytrenko et al. 2025), we remove from the sample all stars satisfying any of the following criteria:

$$\begin{aligned} \text{RUWE} &> 1.4, \\ \frac{\varpi}{\sigma_\varpi} &< 5, \quad \text{if } R \leq 15 \text{ kpc}, \\ \varpi &> 0, \quad \text{if } R > 15 \text{ kpc}, \\ |V_Z| &> 100 \text{ km s}^{-1}. \end{aligned} \quad (1)$$

The parallaxes of stars in the sample were corrected following the prescriptions of Lindegren et al. (2021), using the Z5 and Z6 parallax-bias terms. For stars with absolute magnitudes  $M_G$  between 9 and 13, we also correct the proper motions using the recommendations of Cantat-Gaudin & Brandt (2021). In addition, we remove the magnitude-dependent trend in radial velocities according to the prescription of D. Katz (*Gaia* DR3 documentation). For stars with `rv_template_teff`  $< 8500 \text{ K}$ , we subtract from the reported *Gaia* radial velocity the correction

$$V_{\text{corr}} = \begin{cases} 0, & \text{if } \text{grvs\_mag} < 11, \\ 0.02755 g^2 - 0.55863 g + 2.81129, & \text{if } g \geq 11, \end{cases} \quad (2)$$

where  $g \equiv \text{grvs\_mag}$  and  $V_{\text{corr}}$  is given in  $\text{km s}^{-1}$ .

After applying the quality cuts and corrections mentioned above, the final RGB sample contains 4 547 980 stars with full space velocities. This sample is used in all subsequent calculations, including the determination of both the Galactic rotation curve and the circular velocity curve.

## 3 COORDINATE SYSTEMS

We introduce a local, right-handed Cartesian coordinate system  $(x, y, z)$  at any arbitrary point in the Galactic disc, analogous to the Galactic rectangular system  $(X, Y, Z)$ . This is possible because for any given point (e.g., a star) and for the stars located in its neighbourhood the spatial coordinates and velocity components are known. The transformation from the Galactic Cartesian system to a local Cartesian system is equivalent to placing a fictitious observer at the position corresponding to the Galactic coordinates of the local system's origin.

To ensure consistency between the  $(X, Y, Z)$  Cartesian system and the Galactocentric cylindrical system  $(R, \Theta, Z)$ , Fig. 1, we adopt the Solar distance from the Galactic centre of  $R_\odot = 8.122$  kpc obtained by GRAVITY Collaboration et al. (2021), and the Solar velocity components  $(U_\odot, V_\odot, W_\odot) = (11.1, 245.8, 7.8) \text{ km s}^{-1}$  (Reid & Brunthaler 2004).

The local Cartesian coordinate system is defined in such a way that its  $x$ -axis always points from the centroid towards the Galactic rotation centre, the  $y$ -axis coincides with the direction of Galactic

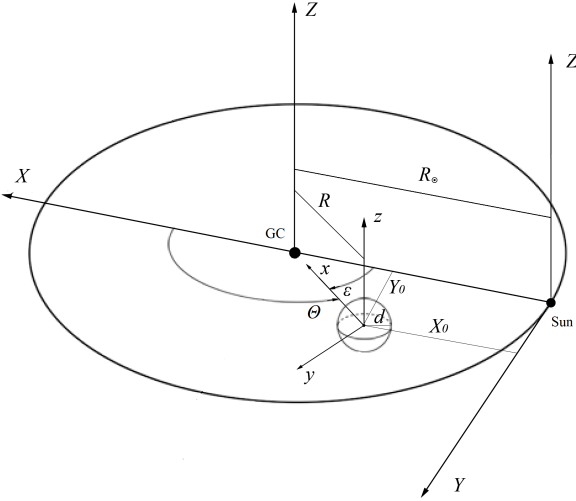


**Figure 1.** The link between the Galactocentric, Galactic and local coordinate systems.

rotation, and the  $z$ -axis is parallel to the direction from the Galactic center to its north pole.

The ‘observation points’ from which the fictitious observer samples the stellar velocities are defined as follows. For stars with relative parallax errors smaller than 20 per cent and Galactocentric distances less than 15 kpc, we construct spherical volumes of radius 1 kpc. The centres of these spheres are placed at the nodes of a rectangular grid located in the Galactic mid-plane, i.e. all grid nodes satisfy  $Z = 0$ . The grid spacing in both  $X$  and  $Y$  directions is 100 pc. For stars at Galactocentric distances larger than 15 kpc, we apply the condition  $\varpi > 0$ . All stars within each spherical region are used to form a stellar system whose centroid velocity is defined as the mean velocity of the stars in that sphere. Thus, our sample was always limited by the condition  $|Z| < 1$  kpc. The same stellar systems are constructed in the planes  $Z = -1$  kpc,  $Z = -0.5$  kpc,  $Z = 0.5$  kpc and  $Z = 1$  kpc. This allows us to determine the velocities above and below the Galactic plane, specifically at  $Z = \pm 0.5$  kpc.

#### 4 VELOCITY MAPS AND DETERMINATION OF THE GALACTIC ROTATION CURVE

The rotation curves  $V_\Theta(R)$  derived from observations of externally perturbed stellar systems do not coincide with the circular velocity  $V_c(R)$  because of the presence of asymmetric drift. Recovering the true circular velocity requires applying an appropriate correction, which is often difficult to determine reliably. Even when such a correction can be attempted, it is not derived from direct measurements, but rather from model reconstructions based on azimuthally averaged line-of-sight velocities and assumptions about the shape of the dispersion profile and the degree of anisotropy. Therefore, in a number of applications, for example in the task of identifying Milky Way analogues (e.g. Vavilova et al. 2024; Kompaniits et al. 2025), it is more appropriate to compare the directly observed rotation curve  $V_\Theta(R)$  of the Milky Way disc with the always-observable rotation curves of external edge-on galaxies.

Because our goal is to study the velocity field over an extended region of the Galactic plane, accurate distance estimates are required. In practice, the distances (parallaxes) in *Gaia* DR3, particularly for stars with large parallax uncertainties, must be refined. To minimize

reliance on model assumptions, we use approaches based as far as possible on purely observational or geometric reasoning. We examine several methods for obtaining the most accurate distance estimates, including direct inversion of *Gaia* parallaxes and the Lucy deconvolution method (Lucy 1974). Direct inversion produces significantly distorted Galactocentric distances already at  $R \gtrsim 12$ –13 kpc.

The Lucy inversion technique has been applied in several studies, including López-Corredoira & Sylos Labini (2019); Chrobáková et al. (2020); Wang et al. (2023). According to the authors, the method reduces parallax errors, increases the number of sources used, and extends the distances that can be reached. In other works, spectrophotometric distances were employed: Eilers et al. (2019) and Ou et al. (2024) used such distances for more than 30 000 RGB stars. Zhou et al. (2023) used a similar approach for  $\sim 54$  000 thin-disc stars, although with a different set of priors. Nearly all other approaches rely, to some extent, on priors and approximate Galactic models to infer distance probabilities.

Our analysis showed that, for our purposes, the most suitable distance estimates are those obtained using the parallax-bias correction proposed by Lindegren et al. (2021), i.e.

$$\varpi_{\text{corr}} = \varpi_{\text{obs}} - Z_5 - Z_6, \quad (3)$$

where  $Z_5$  and  $Z_6$  are the recommended color- and magnitude-dependent bias terms.

To determine the post-correction parallax uncertainty, we adopt

$$\sigma_{\varpi, \text{corr}}^2 = \sigma_{\varpi, \text{obs}}^2 + \sigma_{\text{sys}}^2, \quad (4)$$

where  $\sigma_{\varpi, \text{obs}}$  is the formal *Gaia* DR3 parallax uncertainty, and  $\sigma_{\text{sys}} \approx 10 \mu\text{as}$  represents the external systematic uncertainty (Maíz Apellániz et al. 2021; Maíz Apellániz 2022; Ding et al. 2025).

The heliocentric distance is computed as

$$d = \frac{1}{\varpi_{\text{corr}}}, \quad (5)$$

and its uncertainty follows from error propagation:

$$\sigma_d = \frac{\sigma_{\varpi, \text{corr}}}{\varpi_{\text{corr}}^2}. \quad (6)$$

Using these values, and transforming from  $(d, \mu_\alpha, \mu_\delta, V_r)$  to the Galactocentric cylindrical components  $(V_R, V_\Theta, V_Z)$ , as well as converting  $(\sigma_d, \sigma_{\mu_\alpha}, \sigma_{\mu_\delta}, \sigma_{V_r})$  into  $(\sigma_{V_R}, \sigma_{V_\Theta}, \sigma_{V_Z})$ , we obtain individual Galactocentric velocities and associated uncertainties for each star.

As in Fedorov et al. (2023), the centroid velocities  $V_R$ ,  $V_\Theta$ , and  $V_Z$  and the nine remaining kinematic parameters of the linear Ogorodnikov–Milne model (Ogorodnikov 1965) were computed from the individual stellar velocities contained within each bin (a sphere of radius 1 kpc). The resulting Galactocentric cylindrical velocity components of the centroids are shown in Figs. 2, 3, 4 as functions of Galactocentric coordinates, after applying the parallax corrections described above.

#### 5 DETERMINATION OF THE GALACTIC CIRCULAR VELOCITY FROM THE JEANS EQUATION

In this work, we derive the Galactic rotation curve using purely kinematic quantities that are free from model assumptions. Nevertheless, because the Milky Way is observed from the inside, the reconstruction of the circular velocity  $V_c(R)$  inevitably requires modeling. From the interior of the Galaxy one can determine the full three-dimensional velocities of individual stars, making it possible to recover, via the Jeans equation, a rotation curve of unmatched

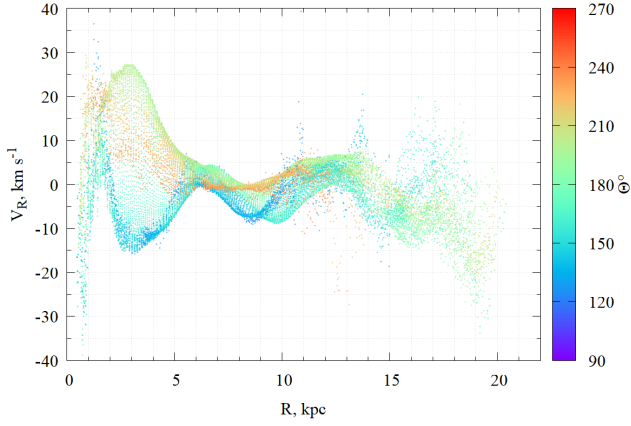


**Figure 2.** The centroid velocity component  $V_R$  as a function of Galactocentric coordinates.

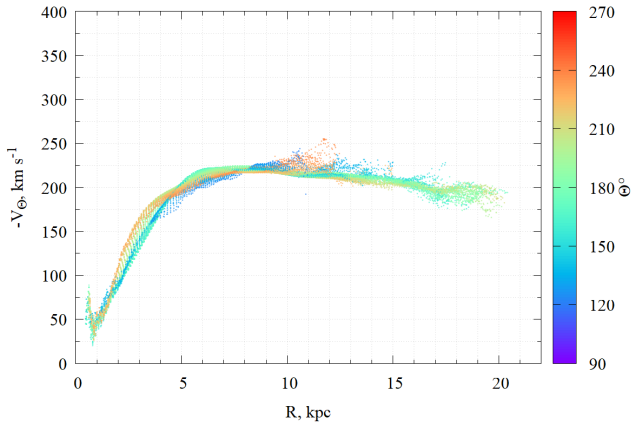


**Figure 3.** The centroid velocity component  $V_\Theta$  as a function of Galactocentric coordinates.

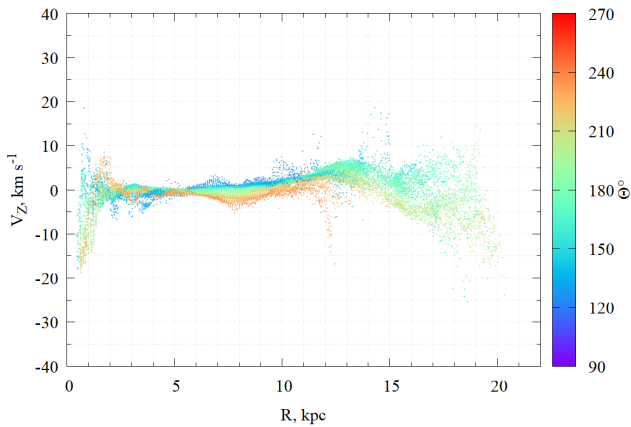


**Figure 4.** The centroid velocity component  $V_Z$  as a function of Galactocentric coordinates.

precision and spatial detail out to  $\sim 25$  kpc (Ou et al. 2024; Zhou et al. 2023; Wang et al. 2023; Jiao et al. 2023; Koop et al. 2024). Such rotation curves provide not only constraints on the total mass of the Galaxy, but also serve as key diagnostics when identifying Milky Way analogues. However, as recently shown by Koop et al. (2024), axisymmetric stationary Jeans modeling becomes unreliable at large radii, requiring caution when interpreting the circular velocity in the outer regions.

To derive the circular velocity curve and study its azimuthal variations, we use the same stellar sample and the same selection criteria as described in the previous section, adding a few additional requirements. In a given gravitational potential  $\Phi(R, z)$  one can compute the velocity an object would have if it were moving on a perfect circular orbit of radius  $R$ , where the gravitational force is balanced by the centrifugal force. To determine this velocity, we use the radial Jeans equation in cylindrical coordinates  $(R, \Theta, z)$  (Binney & Tremaine 2008):

$$\frac{\partial(\nu \langle v_R^2 \rangle)}{\partial R} + \frac{\partial(\nu \langle v_R v_Z \rangle)}{\partial z} + \nu \left( \frac{\langle v_R^2 \rangle - \langle v_\Theta^2 \rangle}{R} \right) = -\nu \frac{\partial \Phi}{\partial R}, \quad (7)$$

where  $\nu(R, Z)$  is the tracer density, and angle brackets denote ensemble averages.

The radial gravitational force in equation (7) is related to the circular velocity by

$$V_c^2(R, z) = R \frac{\partial \Phi}{\partial R}. \quad (8)$$

This quantity is the mathematically defined speed of an ideal circular orbit at a given radius. It is not a directly observable velocity, but a model-based quantity tied to the mass distribution of the Galaxy (including dark matter). The term ‘ideal’ emphasizes that this is not a measurable quantity, but the velocity which the star would have if it were moving in a circular orbit without any perturbations. In reality, the observed velocity and the circular velocity do not coincide. The difference between them contains information about the Galactic dynamics and the mass distribution. Equation 7 shows that the radial force is balanced by the presence of the second moments of the velocity distribution and the tracer density.

Equation 7 assumes that  $\Phi(R, z)$  is the galactic axisymmetric potential,  $R$  is the radius of the Galaxy,  $v_R$  is the radial velocity,  $v_\Theta$  is the azimuthal velocity,  $v_Z$  is the vertical velocity, and angle brackets  $\langle \cdot \rangle$  denote the average value of a given quantity.

Following previous works of Ou et al. (2024); Bland-Hawthorn & Gerhard (2016), we represented the population density distribution of tracers  $\nu(R, z)$  by an analytical function of the form:

$$\nu(R, z) \propto \exp\left(-\frac{R}{h_R}\right) \exp\left(-\frac{|z|}{h_z}\right), \quad (9)$$

with scale length  $h_R = 3$  kpc and scale height  $h_z = 0.3$  kpc.

To derive the circular velocity curve from the Jeans equation 8, we rewrite it as

$$V_c^2 = \langle v_\Theta^2 \rangle - \langle v_R^2 \rangle + R \left[ \frac{1}{\nu} \frac{\partial(\nu \langle v_R^2 \rangle)}{\partial R} + \frac{1}{\nu} \frac{\partial(\nu \langle v_R v_Z \rangle)}{\partial z} \right]. \quad (10)$$

Then, rewriting this equation with gradients in  $R$  and  $Z$  in logarithmic form

$$V_c^2(R, z) = \langle v_\Theta^2 \rangle - \langle v_R^2 \rangle + R \left[ \frac{\partial \langle v_R^2 \rangle}{\partial R} + \langle v_R^2 \rangle \frac{\partial \ln \nu}{\partial R} + \frac{\partial \langle v_R v_Z \rangle}{\partial z} + \langle v_R v_Z \rangle \frac{\partial \ln \nu}{\partial z} \right], \quad (11)$$



and substituting into it the expression for  $v(R, Z)$ , we obtain the final expression for the circular velocity in a form convenient for calculation:

$$V_c^2(R, z) = \langle v_\Theta \rangle^2 + \sigma_\Theta^2 + (\langle v_R \rangle^2 + \sigma_R^2) \left( \frac{R - h_R}{h_R} \right) - 2R \langle v_R \rangle \frac{\partial \langle v_R \rangle}{\partial R} - R \frac{\partial \sigma_R^2}{\partial R} + \frac{R}{h_z} \frac{z}{|z|} \langle v_R v_Z \rangle - R \frac{\partial \langle v_R v_Z \rangle}{\partial z} \quad (12)$$

where  $\langle v^2 \rangle$  is the average value of the squared velocity for each component, which for a specific bin, i.e. a sphere with radius  $d = 1$  kpc, can be written as:

$$\langle v^2 \rangle = \langle v \rangle^2 + \sigma^2 + \sigma_{\text{obs}}^2, \quad (13)$$

where  $\sigma^2$  is the intrinsic velocity dispersion in the bin,  $\langle v \rangle$  the mean velocity, and  $\sigma_{\text{obs}}^2$  the propagated measurement variance transformed into the Galactocentric system. The second term in equation (11) is the asymmetric-drift correction, while the third term represents the cross-term contribution. Equation (11) requires no assumptions other than the tracer-density model itself.

When transforming the observed mean azimuthal velocity  $\langle v_\Theta \rangle$  into the circular velocity  $\langle v_c \rangle$ , the quantities  $\langle v_R^2 \rangle$ ,  $\langle v_\Theta^2 \rangle$ ,  $\langle v_Z^2 \rangle$  and  $\langle v_R v_Z \rangle$  determine the ‘anisotropy correction’ of the velocity field, i.e. how different the stellar velocity dispersions are in the radial, azimuthal and vertical directions. In the cylindrical coordinates  $(R, \Theta, Z)$ , the anisotropy is usually characterized by ratios of dispersions, which form the velocity ellipsoid parameters. By computing the second-order moments (dispersions and covariances) of stellar velocities, we construct the full dispersion tensor, which characterizes the spatial orientation and shape of the velocity ellipsoid:

$$C_{\text{obs}} = \begin{pmatrix} \sigma_{v_R}^2 & \sigma_{v_R v_\Theta} & \sigma_{v_R v_Z} \\ \sigma_{v_\Theta v_R} & \sigma_{v_\Theta}^2 & \sigma_{v_\Theta v_Z} \\ \sigma_{v_Z v_R} & \sigma_{v_Z v_\Theta} & \sigma_{v_Z}^2 \end{pmatrix}. \quad (14)$$

The described algorithm for computing dispersion-tensor components using a spherical bin allows us to obtain, for each bin, a well-defined dispersion value associated with the centroid coordinates  $(R_i, \Theta_i)$ . This sets us free from the need to approximate them with analytic functions. However, real velocity fields are non-stationary and non-uniform. For example,  $v_R$  inside a bin systematically depends on radius  $R$  (e.g. due to density waves or large-scale streaming flows). Within a bin, the radius can vary by up to 2 kpc, which already results in systematic differences of tens of  $\text{km s}^{-1}$ . Therefore, even after subtracting the mean velocity, residual gradients are still present and contribute to the measured dispersions that are not “noise” in the statistical sense. Thus, the measured dispersion is a mixture:

$$\sigma_{\text{measured}}^2 = \sigma_{\text{true}}^2 + \sigma_{\text{gradient}}^2 + \sigma_{\text{stream}}^2. \quad (15)$$

For this reason, instead of simply averaging the velocities in each spherical region, we determine all 12 kinematic parameters of the Ogorodnikov–Milne model (Fedorov et al. 2023). The difference between the observed stellar velocity and the model prediction (the O–M equation residuals) is treated as a residual velocity whose distribution in each cell becomes close to Gaussian. These residual velocities represent the peculiar stellar velocities affected by measurement errors.

To compute the dispersions of these peculiar velocities, we use for each star the measured values (with corrected parallax)  $(d, \mu_\alpha, \mu_\delta, v_r)$  and their uncertainties  $(\sigma_d, \sigma_{\mu_\alpha}, \sigma_{\mu_\delta}, \sigma_{v_r})$ , obtained from the *Gaia* astrometry, and transform them into the required coordinate system. If one simply takes the residual velocities and computes the dispersion, the result contains both the true peculiar-velocity

dispersion and the measurement noise. Therefore, we compute the dispersions not directly but using the covariance matrices of the propagated measurement errors.

For each star, we construct a  $3 \times 3$  covariance matrix of the propagated velocity uncertainties:

$$E_i = \begin{pmatrix} e_{v_R}^2 & e_{v_R v_\Theta} & e_{v_R v_Z} \\ e_{v_\Theta v_R} & e_{v_\Theta}^2 & e_{v_\Theta v_Z} \\ e_{v_Z v_R} & e_{v_Z v_\Theta} & e_{v_Z}^2 \end{pmatrix}, \quad (16)$$

The elements of this matrix were obtained by linearly propagating the errors of the astrometric parameters using the Jacobian  $J_i$  and  $C_{\text{astro}, i}$  is the covariance matrix of the errors of the astrometric measurements from *Gaia*. Formally:

$$E_i = J_i C_{\text{astro}, i} J_i^T, \quad (17)$$

All matrices  $E_i$  in the bin are averaged and the ‘true’ covariance tensor is obtained after subtracting the contribution of the measurement noise:

$$C_{\text{true}} = C_{\text{obs}} - \langle E \rangle, \quad (18)$$

yielding the corrected values of  $\sigma_{v_R}$ ,  $\sigma_{v_\Theta}$ ,  $\sigma_{v_Z}$  and  $\sigma_{v_R v_Z}$ .

In this way, we “cleanse” the dispersion tensor from the contribution of measurement errors and obtain the corresponding values  $(\sigma_{v_R}, \sigma_{v_\Theta}, \sigma_{v_Z}, \text{ and } \sigma_{v_R v_Z})$ . The figure 5 shows  $(\sigma_{v_R}, \sigma_{v_\Theta}, \sigma_{v_Z}, \text{ and } \sigma_{v_R v_Z})$  obtained in the Galactic plane as functions of distance  $R$ .

When computing  $V_c$  through equation 11, derivatives of the form  $\partial \langle v_R^2 \rangle / \partial R$ ,  $\partial \langle v_R v_Z \rangle / \partial Z$  appear, which need to be determined. Taking these derivatives directly from observational data yields a ‘jagged’ dispersion profile due to noise, sample sparseness, and distance errors. To reduce noise, we did not approximate the dispersions with analytical functions, but instead calculated numerical derivatives based on dispersion values at points spaced 100 pc apart and contained within each sphere of radius  $R = 1$  kpc. Unfortunately, this did not radically reduce noise, but it did provide the opportunity to rely on real, unsmoothed data and eliminate the need for model representations. The derived quantities were then substituted into the Jeans equation to obtain the circular velocity  $V_c(R)$  in each spherical region of radius 1 kpc. The dependence of  $V_c$  on Galactocentric radius at  $\Theta = 180^\circ$  is shown in Fig. 7.

Figure 6 shows  $V_c$  and  $V_\Theta$  as a function of Galactocentric distance  $R$ . To make the comparison easier, the three panels display the functions corresponding to stars contained within spheres centered at  $Z = -1.0$  and  $-0.5$  kpc (left),  $Z = 0.0$  kpc (middle) and  $Z = 1.0$  and  $0.5$  kpc (right). Each point on the figure represents the value of  $V_c$  and  $V_\Theta$  in specific spheres ( $R = 1$  kpc), separated by 100 pc. Averaging over  $\Theta$  is performed in the range of  $150^\circ - 210^\circ$ .

The rotation curve looks smoother than the circular velocity curve. However, despite some fluctuations in  $V_c$ , the general trend, a decrease in velocity with distance, is clearly observed. At the same time, it is clearly visible that the curves differ somewhat in their slope, especially at large distances. The difference in amplitude is approximately  $15 - 25 \text{ km s}^{-1}$ . According to Fig. 7, the  $V_c$  and  $V_\Theta$  curves are not linear functions in the distance range of  $6 - 20$  kpc. Therefore, approximating their slope with a straight line seems inappropriate. Although in general (on average) the slopes of both curves are consistent, starting from about 16 kpc, we see that the overall slope of our curves is noticeably greater than that of the curve from Eilers et al. (2019). We also note that the value of our circular velocity up to 15 kpc almost coincides with the values of Eilers et al. (2019), although our curve is much more detailed.

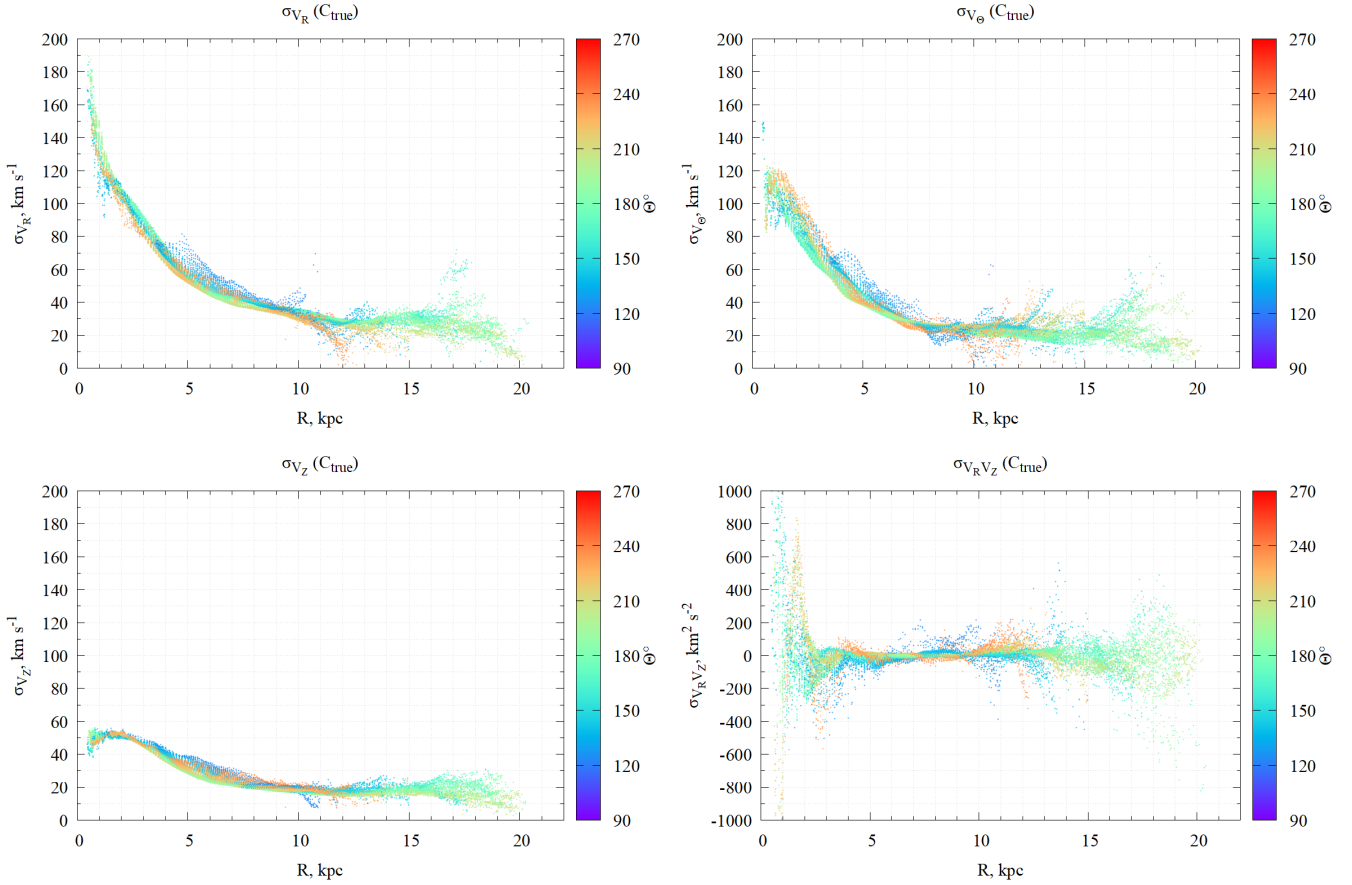


**Figure 5.**  $\sigma v_R$ ,  $\sigma v_\Theta$ ,  $\sigma v_Z$  and  $\sigma v_R v_Z$  as functions of Galactocentric coordinates.

## 6 CIRCULAR VELOCITY VERSUS GALACTIC AZIMUTH AND ROTATION CURVES IN Z-LAYERS

We analyze the behavior of  $V_c$  and  $V_\Theta$  over the range of  $\Theta$  angles from  $150^\circ$  to  $210^\circ$ . Figures 8, 9 show the velocities as a function of  $R$  and  $\Theta$ . The plots are shown for negative heights on the left and for positive heights on the right.

The circular velocity is presented only in Fig. 9, since only the Galactic mid-plane is the plane of dynamical symmetry of the potential. Figs. 8 show the centroid velocities at various height layers. These velocities are not referred to the Galactic mid-plane, but to a certain ‘effective plane’ by the heights of the centroids.

Figure. 10 shows the heights of the centroids as a function of distance for different  $Z$ . The tilts are caused by several physical factors that prevent us from interpreting  $V_c$  as a classical circular velocity. These ‘circular velocities’ in the figure represent rotation curves for a population with average  $Z$  and reflect the kinematics of a mixture of the thin and thick disks, and part of the halo at large  $R$ . Essentially, their behavior reflects the influence of the transition from disk to halo, the influence of the vertical structure of the potential and asymmetric drift as a function of  $R$  and  $Z$ , as well as the influence of disk oscillations and warp. This is the physical meaning of the presented quantities, and it does not coincide at all with the physical meaning of the circular velocity for the thin disk. It is clearly seen from the figure that in the Galactic plane, no significant difference between the dependencies at different azimuths is observed up to  $\sim 15$  kpc. However, starting at  $15$ – $16$  kpc, the differences become large not

only in the Galactic plane but also at various  $Z$ -heights, indicating a more complex velocity field in the  $(R, z)$  plane compared to the inner disk. Since most studies refer to the circular velocity curve from Eilers et al. (2019) and often make comparisons with it, we also show this function in blue in all figures.

It is clearly seen that  $V_c$ , obtained by averaging in the range of azimuthal angles  $\pm 30^\circ$ , is significantly closer to the blue dots (the curve from Eilers et al. 2019). This likely indicates that the curve in Eilers et al. (2019) was obtained by averaging over all azimuths available.

## 7 SUMMARY AND CONCLUSIONS

First, we note that the results obtained do not contradict other published findings (e.g., Eilers et al. 2019; Ou et al. 2024; Wang et al. 2023; Koop et al. 2024, and others). At the same time, it should be emphasized that they were derived from an RGB sample (4,547,980 stars) taken solely from *Gaia* DR3, with minimal reliance on model-based data. In addition, the circular and rotational velocity curves are highly detailed, as they were constructed using spatial nodes separated by only 100 pc. The resulting rotation curve and circular velocity curve exhibit some features not always observed in other studies. These features are present at distances of  $\sim 13$  and  $\sim 18$  kpc. However, they can sometimes be found in other studies, albeit in a significantly smoother form (see, for example, Koop et al. 2024). To verify whether the dip at 18 kpc is real, we constructed a rotation

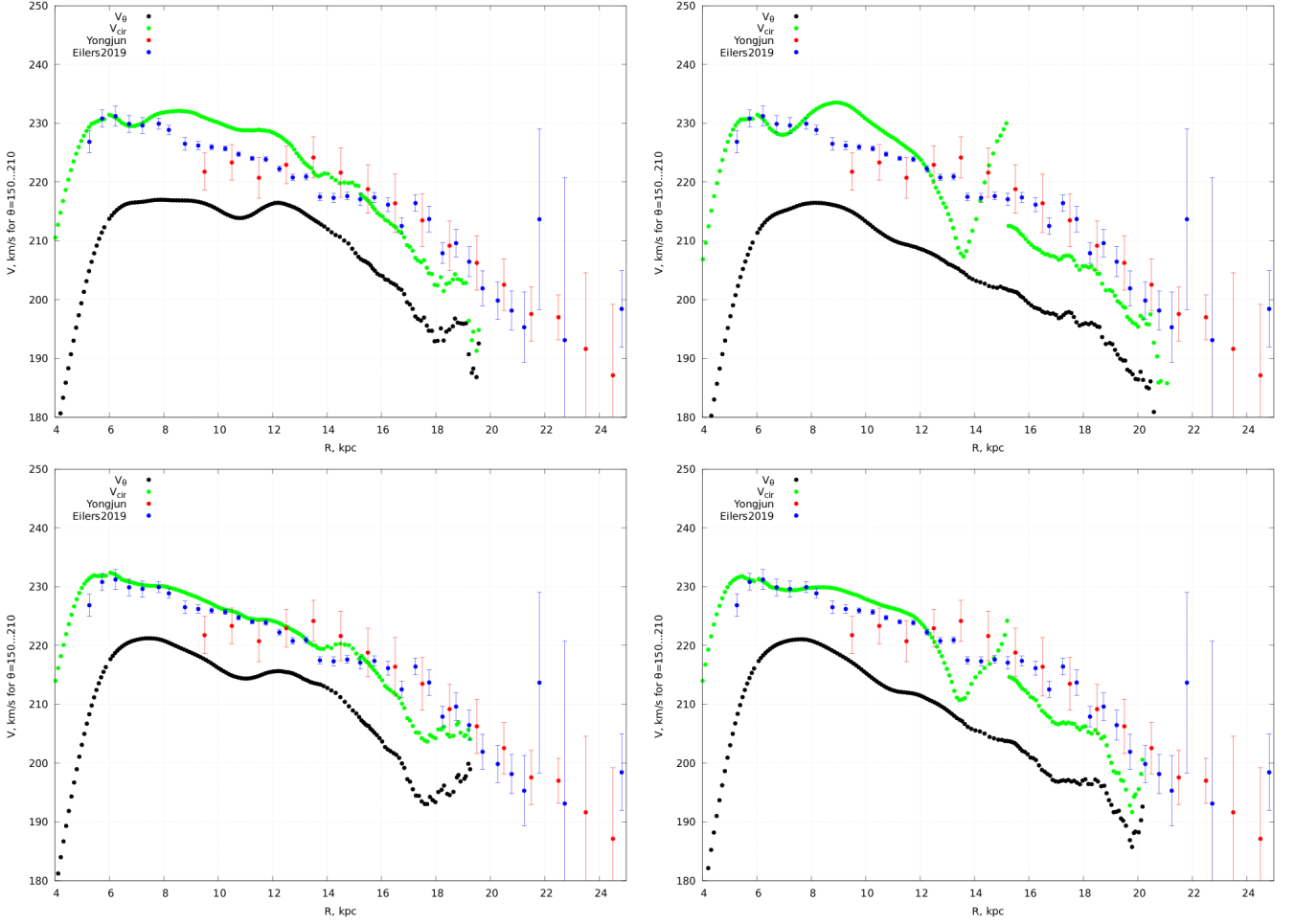


**Figure 6.** Averaged  $V_c$  and  $V_\theta$  as a function of the Galactocentric distance along the direction  $\Theta = 180^\circ$ , determined from stars contained in spheres with centers located at  $Z \pm 1.0$  and  $Z \pm 0.5$  kpc. Averaging of  $V_c$  and  $V_\theta$  was performed in the ranges of azimuthal angles  $\pm 30^\circ$  with respect to  $\Theta = 180^\circ$ .

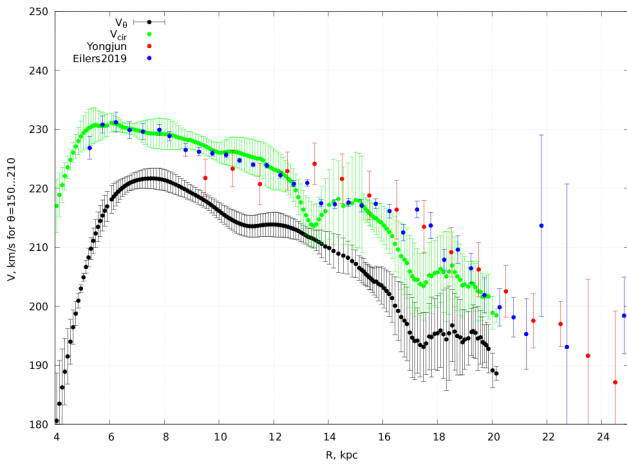


**Figure 7.** Averaged  $V_c$  and  $V_\theta$  as a function of the Galactocentric distance along the direction  $\Theta = 180^\circ$ , determined from stars contained in spheres with centers located at  $Z = 0.0$  kpc. Averaging of  $V_c$  and  $V_\theta$  was performed in the ranges of azimuthal angles  $\pm 30^\circ$  with respect to  $\Theta = 180^\circ$ .

curve for our sample using the photogeometric distances obtained by [Bailer-Jones et al. \(2021\)](#) as a distance estimate.

A noticeable velocity decrease turned out to be also present at radii of  $\sim 13 - 18$  kpc. Some discrepancy in the specific distance values where the velocity minimum is reached is apparently due to the use of different distance estimates. Therefore, the noticeable decrease in rotation velocity near these points is, in our opinion, real and is not determined by parallax inaccuracies, but rather indicates the presence of a rather complex velocity field at this radius.

When approximating the derived circular velocity with a linear function, we see a steady decrease in the circular velocity by  $2.3 \pm 0.5$   $\text{km s}^{-1} \text{ kpc}^{-1}$  over the entire range of distances used, which can be represented as:

$$V_c(R_\odot) = (229.63 \pm 0.30) \text{ km s}^{-1} - (2.29 \pm 0.05) \text{ km s}^{-1} \text{ kpc}^{-1} \cdot (R - R_\odot)$$

This is consistent with previous studies by [Wang et al. \(2023\)](#); [Zhou et al. \(2023\)](#); [Ou et al. \(2024\)](#) and [Jiao et al. \(2023\)](#).

We observe rotation curves that are not quite identical at different  $\Theta$  angles, indicating a dependence of the circular velocity on azimuth. Although the differences are small, they do exist and are particularly noticeable at large  $\Theta$  angles, where they can reach  $\sim 20$   $\text{km s}^{-1}$  and be completely different from the curve at  $\Theta = 180$ . In this sense, we regard a given circular velocity curve as a local characteristic, the

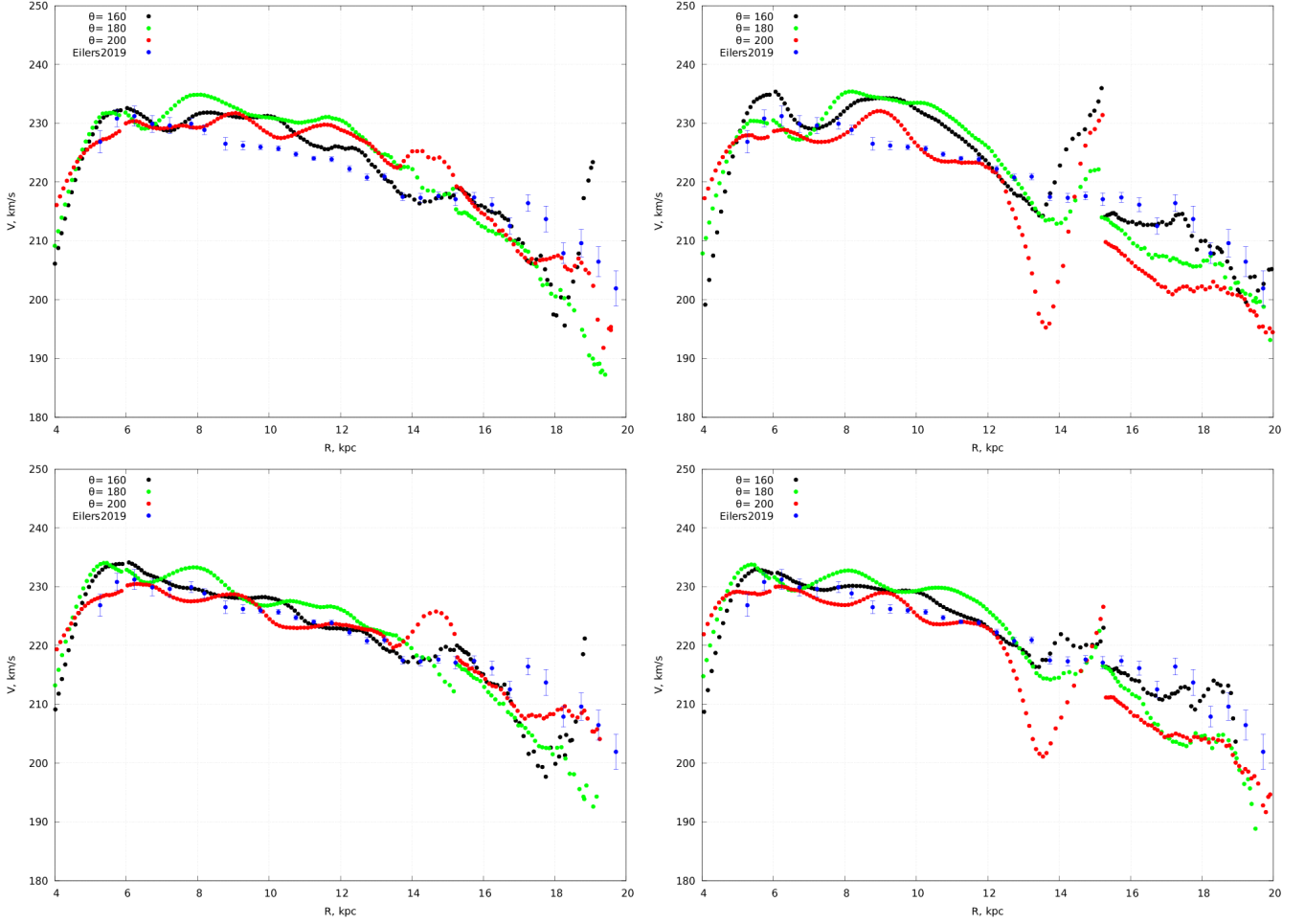


**Figure 8.** The velocity  $V$  as a function of Galactocentric distance along various azimuthal directions at heights  $Z = \pm 0.5$  and  $\pm 1.0$  kpc. The dependences were obtained for  $\Theta = 160^\circ$ ,  $180^\circ$ , and  $200^\circ$  by averaging them over azimuthal angle ranges of  $\pm 10^\circ$  relative to each specified  $\Theta$ .

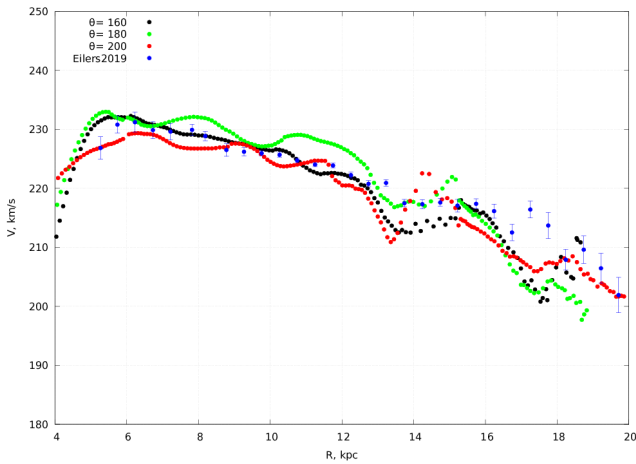


**Figure 9.** The velocity  $V$  as a function of Galactocentric distance along various azimuthal directions at heights  $Z = 0$  kpc. The dependences were obtained for  $\Theta = 160^\circ$ ,  $180^\circ$ , and  $200^\circ$  by averaging them over azimuthal angle ranges of  $\pm 10^\circ$  relative to each specified  $\Theta$ .

application of which to the entire Galaxy seems unjustified to us. The lack of data for a significantly wider range of  $\Theta$  angles and the limited distance range require great caution in determining the shape of the  $V_c$  curve and its derivative  $dV_c/dR$ , especially for determining the Galactic mass. However, the use of detailed  $V_c$  and  $V_\Theta$ , along with additional indicators, e.g. morphology, composition, etc., may prove effective characteristics for use as indicators of Milky Way analogues.

## 8 ACKNOWLEDGEMENTS

This work has made use of data from the European Space Agency (ESA) mission *Gaia* (<https://www.cosmos.esa.int/gaia>), processed by the *Gaia* Data Processing and Analysis Consortium (DPAC, <https://www.cosmos.esa.int/web/gaia/dpac/consortium>). Funding for the DPAC has been provided by national institutions, in particular the institutions participating in the *Gaia* Multilateral Agreement.

This work is supported by the National Research Foundation of Ukraine, Project No. 2023.03/0188 (Vavilova et al. 2024), and the Ministry of Education and Science of Ukraine.



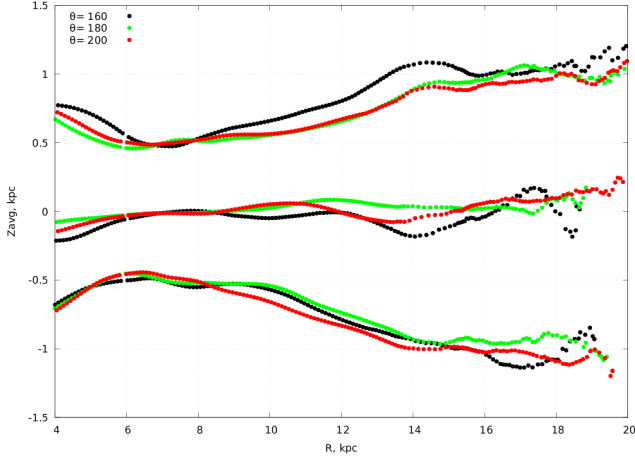


**Figure 10.** The heights of the centroids as a function of Galactocentric distance with the centers of the spheres located at  $Z = -1$ ,  $Z = 0$ , and  $Z = 1$  kpc.

## DATA AVAILABILITY

The used catalogue data are available in a standardized format for readers via the CDS (<https://cds.u-strasbg.fr>). The software code used in this paper can be made available on personal request by e-mail: [akhmetovvs@gmail.com](mailto:akhmetovvs@gmail.com).

## REFERENCES

- Akhmetov V. S., Bucciarelli B., Crosta M., Lattanzi M. G., Spagna A., Re Fiorentin P., Bannikova E. Y., 2024, *MNRAS*, **530**, 710
- Andrae R., et al., 2023, *A&A*, **674**, A27
- Antoja T., et al., 2018, *Nature*, **561**, 360
- Bailer-Jones C. A. L., Rybizki J., Fouesneau M., Demleitner M., Andrae R., 2021, *AJ*, **161**, 147
- Binney J., Tremaine S., 2008, *Galactic Dynamics: Second Edition*. Princeton University Press
- Bland-Hawthorn J., Gerhard O., 2016, *ARA&A*, **54**, 529
- Cantat-Gaudin T., Brandt T. D., 2021, *A&A*, **649**, A124
- Chrobáková Ž., López-Corredoira M., Sylos Labini F., Wang H.-F., Nagy R., 2020, *A&A*, **642**, A95
- Denyshchenko S. I., Fedorov P. N., Akhmetov V. S., Velichko A. B., Dmytrenko A. M., 2024, *MNRAS*, **527**, 1472
- Ding Y., Liao S., Wen S., Qi Z., 2025, *AJ*, **169**, 211
- Dmytrenko A. M., Fedorov P. N., Akhmetov V. S., Velichko A. B., Denyshchenko S. I., 2023, *MNRAS*, **521**, 4247
- Dmytrenko A. M., et al., 2025, *MNRAS*, **542**, 2542
- Eilers A.-C., Hogg D. W., Rix H.-W., Ness M. K., 2019, *ApJ*, **871**, 120
- Fedorov P. N., Akhmetov V. S., Velichko A. B., Dmytrenko A. M., Denyshchenko S. I., 2023, *MNRAS*, **518**, 2761
- GRAVITY Collaboration et al., 2021, *A&A*, **647**, A59
- Gaia Collaboration et al., 2021, *A&A*, **649**, A8
- Gaia Collaboration et al., 2023a, *A&A*, **674**, A1
- Gaia Collaboration et al., 2023b, *A&A*, **674**, A37
- Jiao Y., Hammer F., Wang H., Wang J., Amram P., Chemin L., Yang Y., 2023, *A&A*, **678**, A208
- Kompaniets O. V., et al., 2025, arXiv e-prints, [p. arXiv:2511.18612](https://arxiv.org/abs/2511.18612)
- Koop O., Antoja T., Helmi A., Callingham T. M., Laporte C. F. P., 2024, *A&A*, **692**, A50
- Lindgren L., et al., 2021, *A&A*, **649**, A4
- López-Corredoira M., Sylos Labini F., 2019, *A&A*, **621**, A48
- Lucy L. B., 1974, *AJ*, **79**, 745
- Maíz Apellániz J., 2022, *A&A*, **657**, A130

- Maíz Apellániz J., Pantaleoni González M., Barbá R. H., 2021, *A&A*, **649**, A13
- McMillan P. J., et al., 2022, *MNRAS*, **516**, 4988
- Mróz P., et al., 2019, *ApJ*, **870**, L10
- Ogorodnikov K. F., 1965, *Dynamics of Stellar Systems*. Pergamon Press
- Ou X., Eilers A.-C., Necib L., Frebel A., 2024, *MNRAS*, **528**, 693
- Puglisi A., et al., 2023, *MNRAS*, **524**, 2814
- Reid M. J., Brunthaler A., 2004, *ApJ*, **616**, 872
- Skowron D. M., et al., 2019, *Science*, **365**, 478
- Vasiliev E., Belokurov V., Erkal D., 2021, *MNRAS*, **501**, 2279
- Vavilova I. B., Fedorov P. M., Dobrycheva D. V., Sergijenko O., Vasylenko A. A., Dmytrenko A. M., Khramtsov V. P., Kompaniets O. V., 2024, *Space Science and Technology*, **30**, 81
- Wang H.-F., Chrobáková Ž., López-Corredoira M., Sylos Labini F., 2023, *ApJ*, **942**, 12
- Zhou Y., Li X., Huang Y., Zhang H., 2023, *ApJ*, **946**, 73